

Article

Three-Dimensional Morphology and Watershed-Algorithm-Based Method for Pitting Corrosion Evaluation

Anbang Li ^{1,2,3,*} , Hongwang Ma ¹ and Shanhua Xu ^{1,2,3}¹ School of Civil Engineering, Xi'an University of Architecture & Technology, Xi'an 710055, China² State Key Laboratory of Green Building in Western China, Xi'an 710055, China³ Key Laboratory of Structural Engineering and Earthquake Resistance, Ministry of Education, Xi'an 710055, China

* Correspondence: lianbang@xauat.edu.cn

Abstract: Pitting corrosion and stress concentration at rust pits are the principal reasons for severe degradation in fatigue performance of corroded steel structures. The accurate evaluation of rust pits on rough and uneven corrosion surfaces is the foundation of fatigue life estimation for corroded steel structures. In this paper, a new method for the identification, extraction, and evaluation of rust pits on the surface of corroded steel structures was proposed based on a three-dimensional morphology and watershed algorithm. An accelerated corrosion experiment was first executed to acquire corroded steel plates, and then surface profile measurements were conducted to obtain the three-dimensional morphology of the corroded steel surfaces. Furthermore, the surface topography data of the corroded steel surfaces were written into a gray matrix through coordinate transformation. Then, the gray matrix was successively filtered and gradient-mapped, and the watershed was calculated to obtain the pit mark matrix and pit depth matrix. A calculation method for the size and shape of rust pits was consequently developed, and a statistical analysis of the extraction results of the rust pits was also conducted. The results showed that rust pit density had a peak value at the corrosion duration of 3 months, and rust pit density showed a fluctuating process with corrosion duration that continued to increase until 15 months. The values of the depth diameter ratios of rust pits were concentrated in the range of 0.1~0.8. With corrosion duration increasing from 3 months to 4, 6, 8, 12, and 15 months, the distribution range of the depth diameter ratios of rust pits decreased at first and then increased, followed by decrease and, finally, increase. The width distribution of the rust pits was independent of the depth distribution of the rust pits. The values of the volume ratios were mostly distributed between $\pi/12$ and $\pi/4$, and the shapes of most rust pits were similar to half (ellipsoidal) spheres.

Keywords: corrosion; steel structure; three-dimensional morphology; watershed algorithm; pitting corrosion; rust pit identification

**Citation:** Li, A.; Ma, H.; Xu, S.

Three-Dimensional Morphology and Watershed-Algorithm-Based Method for Pitting Corrosion Evaluation.

Buildings **2022**, *12*, 1908. <https://doi.org/10.3390/buildings12111908>

Academic Editor: Andrea Petrella

Received: 17 October 2022

Accepted: 3 November 2022

Published: 7 November 2022

Publisher's Note: MDPI stays neutral with regard to jurisdictional claims in published maps and institutional affiliations.



Copyright: © 2022 by the authors. Licensee MDPI, Basel, Switzerland. This article is an open access article distributed under the terms and conditions of the Creative Commons Attribution (CC BY) license (<https://creativecommons.org/licenses/by/4.0/>).

1. Introduction

Corrosion is an almost unavoidable durability problem for many steel structures that have been exposed to long-term corrosive environments, such as industry and ocean atmospheres [1,2]. As for corroded steel structures, such as steel bridges, steel crane beams, offshore platforms, etc., that are frequently subjected to fatigue loads, pitting corrosion and stress concentration at rust pits are the principal reasons for severe degradation in fatigue performance of corroded steel structures [3,4]. The meso-characteristics, including the depth, width, area, volume, shape, etc., of rust pits on corroded steel surfaces are the key factors affecting the initiation and propagation of fatigue cracks in corroded steel structures [5–7]. From the aspects of fatigue life prediction and the analysis of corroded steel structures, a common research method is to convert surface rust pits into equivalent initial flaws according to specific equivalence rules; then, fatigue crack propagation prediction can be conducted based on classical fracture mechanics theory [7–11]. Pitting corrosion

evaluation is an important basis for stress concentration analyses, the identification of critical rust pits, and the equivalence of initial cracks for corroded steel structures [12]. Therefore, accurately identifying, extracting, and evaluating the size and shape of rust pits from rough and uneven corrosion surfaces have become key problems in fatigue life estimation for corroded steel structures.

With the development of optical measurement technology, scanning electron microscopy, atomic force microscopy, X-ray tomography, laser confocal microscopy, and white light interference, three-dimensional scanning and other technologies have been applied to the topographic measurement of rust surfaces [13–16], making it possible to accurately analyze rust pits. Wang and Cheng [15] adopted image recognition technology to identify rust pits on corrosion surface images obtained by laser confocal microscopy. The method could better obtain two-dimensional information, such as the position, area, and width of the circular rust pits, but could not determine three-dimensional information, such as the depth and volume of the rust pits. Codaro [17] proposed an image analysis method based on optical microscopy to quantitatively characterize the morphology of rust pits. Automatic image analysis technology was applied by Walde and Hillberry [18], where a random cross-section plan was taken as the quantitative basis of corrosion damage, and the morphology and spatial distribution characteristics of rust pits were analyzed. Wang et al. [19] acquired three-dimensional coordinate data of the surface topography for a corroded steel plate by means of three-dimensional topography scanning, and the location, size, shape, and other parameters of rust pits were then determined using a binary slice image created from top to bottom along the surface height direction. Hlme and Lunder [13] developed an automatic evaluation method for corroded steel surfaces based on white light interferometry. In addition to giving the depth of rust pits, this method could also extract the density, diameter, area, volume, shape, and other parameters of rust pits. However, it should be pointed out that this method was inefficient and only applicable to the fine analysis of early characteristics of pitting corrosion. In general, the main drawbacks of the existing methods of rust pit identification, extraction, and evaluation lie in their low universality and efficiency.

A watershed algorithm is an image segmentation method based on mathematical morphology theory [20]. The basic idea is to take an image as a topographical landform in geodesy, and the gray value of each pixel in the image represents altitude. The mathematical morphology algorithm is applied to find the “watershed”, i.e., the edge of the object that changes rapidly in gray, to achieve image segmentation. Two classical, fast watershed algorithms based on simulated flooding and simulated precipitation, were proposed by Vincent [21] and Smet P D [22], respectively. The watershed algorithm and its improved algorithms have been widely used in image segmentation and recognition in agriculture [23,24], medicine [25,26], remote sensing [27,28], and other fields. Several researchers have also been concerned with watershed-algorithm-based surface defect recognition and extraction [29–31]. To the best of our knowledge, however, there are few studies on the identification and extraction of rust pits on the surfaces of corroded steel structures using watershed algorithms. The traditional watershed image segmentation method starts from a color image. It first turns the color image gray, then calculates a gradient map, and finally calculates the watershed on the basis of the gradient map. Then, it obtains the edge lines of each segmentation part of the image. The accuracy of the traditional watershed image segmentation method is limited by the size of the image pixels, and the graying process of an image can easily cause the loss of detailed information, which may give rise to excessive segmentation of the image. In addition, although the traditional watershed image segmentation method can recognize and extract some two-dimensional information, such as the area, size, and location of rust pits, it is unable to obtain three-dimensional information, such as the depth and shape.

In this paper, a new method for the identification, extraction, and evaluation of rust pits on the surfaces of corroded steel structures is proposed by combining three-dimensional topography-scanning technology and a watershed image segmentation algorithm. An

accelerated corrosion experiment is first executed to acquire corroded steel plates, and then surface profile measurements are conducted to obtain the three-dimensional morphology of the corroded steel surfaces. Furthermore, the elevation data of the corroded steel plate surfaces are directly written into a gray matrix through coordinate transformation to avoid the loss of details of the corrosion surface topography. Then, the gray matrix is successively filtered and gradient-mapped, and the watershed is calculated to obtain a rust pit mark matrix. A rust pit matrix and a contour matrix of the corroded steel structure surfaces are obtained by extracting specific elements of the mark matrix. Finally, the calculation method for the size and shape of rust pits is developed, and a statistical analysis of the extraction results of the rust pits is also conducted. The outcome of this study can provide meaningful references and essential data for the fatigue performance evaluation of existing corroded steel structures.

2. Experiment Procedure

2.1. Accelerated Corrosion Test of H-Beams

An accelerated corrosion test on Q235B hot-rolled H-beams ($HW350 \times 175 \times 7 \times 11$) was carried out by adopting the outdoor periodic automatic spraying of salt spray based on Chinese codes GB/T 24517-2009 [32] and GB/T 10125-2012 [33], as shown in Figure 1. The corrosion medium was a NaCl solution with a concentration of 50 mg/L and a pH value from 6.2 to 7.2. The solution was sprayed every 4 h through an automatic spraying device, and each holding time was 5 min. To study the effect of corrosion duration on the characteristics of rust pits on corroded steel surfaces, seven batches of specimens with corrosion durations of 0, 3, 4, 6, 8, 12, and 15 months, respectively, were designed.



Figure 1. Accelerated corrosion test of H-beams: (a) general view of the test platform and (b) schematic diagram of internal sprinkler.

2.2. Three-Dimensional Morphological Scanning of Corroded Steel Plates

Wire cutting was used to intercept steel plate specimens from the flanges of H-beams with different corrosion durations. An electric wire brush was adopted to clean the rust products on the surfaces of the steel plates until the bottoms of the surface corrosion pits showed a silver-white metallic luster. Anhydrous alcohol was applied to clean residual dust and oil from the corroded steel surfaces. An ST-400 three-dimensional noncontact surface profiler from NANOVEA was adopted to scan the surface profiles of the corroded steel plates. The instrument used the most advanced white light co-aggregation technology to achieve high-resolution surface topography measurements and could collect the three-dimensional coordinate data of each measuring point in real time. The scanning area of the specimens was set to $100 \text{ mm} \times 35 \text{ mm}$ (where 100 mm was the rolling direction and 35 mm was the flange width direction), and the scanning step was 0.1 mm in both the rolling direction and flange width direction. Figure 2 presents the three-dimensional morphology scanning results for the front side of specimen C6, of which the corrosion duration was 6 months.

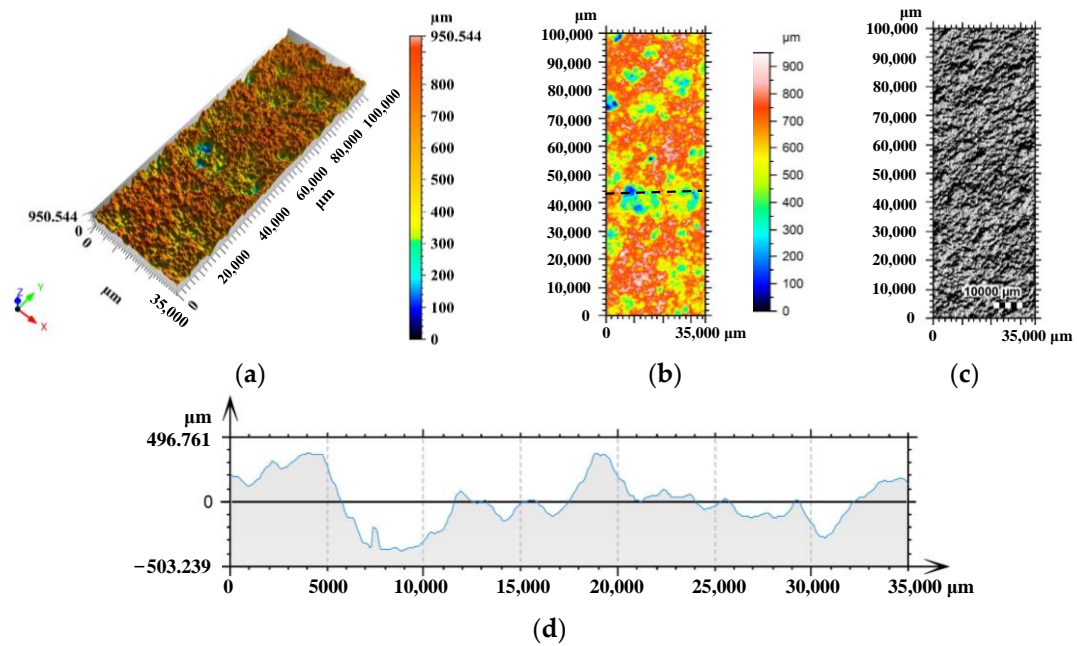


Figure 2. Three-dimensional morphology scanning results for front side of C6: (a) 3D view of the surface, (b) pseudo color view of the surface, (c) photo copy, and (d) profile curve.

3. Identification, Extraction, and Evaluation Method for Rust Pits

The characteristics of corrosion pits include not only dimensional parameters, such as depth, radius, area, and volume, but also shape parameters, such as depth diameter ratio, area ratio, and volume ratio. In this section, a new method for the identification, extraction, and evaluation of rust pits on the surfaces of corroded steel structures is proposed with reference to a traditional image segmentation idea, and the corresponding computational program is also compiled. A block diagram of the program is shown in Figure 3.

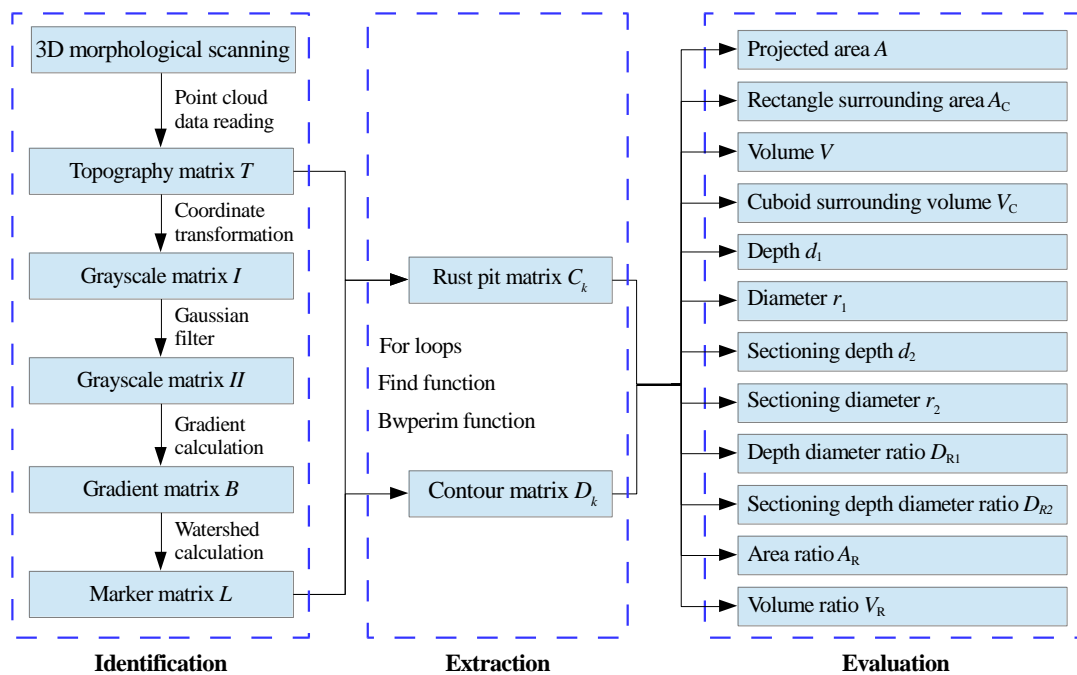


Figure 3. Program chart of identification, extraction, and evaluation of rust pits on the surfaces of corroded steel structures.

3.1. Method of Identifying and Extracting Surface Rust Pits

The surface elevation data of the corroded steel plates obtained by surface topography scanning were directly written into a gray matrix through coordinate transformation to avoid the loss of surface corrosion details. Then, the gray matrix was successively filtered and gradient-mapped, and the watershed was calculated to obtain a mark matrix of the rust pits. Finally, a rust pit matrix and contour matrix were obtained by extracting specific elements of the mark matrix. The detailed process was as follows (programming in MATLAB-based language).

Step 1: Point cloud data reading. The three-dimensional point cloud data obtained by surface morphology scanning of the corroded steel plates were read and stored in a topographic matrix $T(X_N, Y_N, Z_N)$ with N lines \times three columns, as shown in Figure 4a; the three columns of the matrix stored the X, Y, and Z coordinates of each collection point, respectively. X and Y represented the plane position information of each point on the surface of the rusted steel plate in the topography scanning area, and Z represented the height value of each point on the surface of the rusted steel plate relative to the reference plane in the topography scanning area. N represented the total number of points collected in the topography scanning area.

$$N = (L_1/\lambda_1 + 1) \cdot (L_2/\lambda_2 + 1) = (m + 1) \cdot (n + 1) \quad (1)$$

where L_1 and L_2 are the width and length of the topography scanning area, respectively; and λ_1 and λ_2 are the scanning steps in the width and length directions of the topography scanning area, respectively.

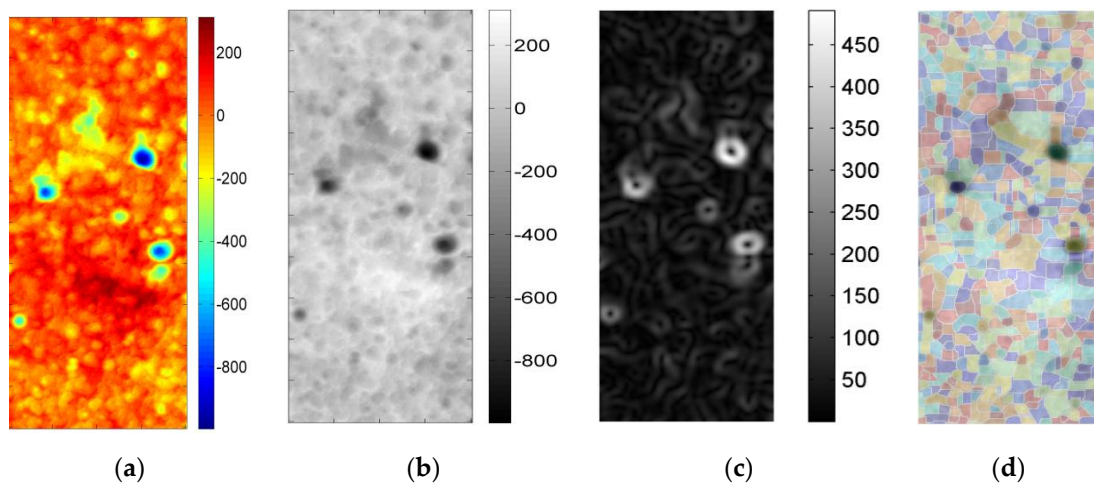


Figure 4. Identification process of rust pits based on watershed algorithm: (a) topography matrix T , (b) gray matrix I , (c) gradient matrix B , (d) mark matrix L .

Step 2: Coordinate transformation. Through plane coordinate transformation, the height of each point on the steel plate surface relative to the reference plane was written into a gray matrix $I(x_n, y_m)$, as shown in Figure 4b, and all the details of the corrosion surface morphology were completely retained in the gray matrix I .

$$I(i, :) = T((i - 1) \cdot (L_1/\lambda_1 + 1) + 1 : i(L_1/\lambda_1 + 1), 3) \quad (2)$$

where $i \in 1 : (L_2/\lambda_2 + 1)$.

Step 3: Gaussian filter. A special function was first used to establish a predefined filter operator w , and then the `imfilter` function was adopted to perform linear smoothing

filtering on the gray matrix I to obtain a new gray matrix II in order to eliminate Gaussian noise and avoid excessive segmentation in the subsequent watershed calculation.

$$II = \text{imfilter}(I, w, \text{'replicate'}) \quad (3)$$

where w is the predefined filter operator.

Step 4: Gradient calculation. The gradient function `Imgradient` was applied to perform gradient calculation on grayscale matrix II , obtaining gradient matrix B of the corroded steel surface, as shown in Figure 4c.

$$B(x, y) = \nabla II(x_i, y_j) \quad (4)$$

where ∇ is the differential operator of two-dimensional vector $\nabla f = \frac{\partial f}{\partial x} \bar{i} + \frac{\partial f}{\partial y} \bar{j}$.

Step 5: Watershed calculation. The Watershed function was applied to carry out watershed calculation for gradient matrix B to obtain the rust pit mark matrix L . As shown in Figure 4d, where the zero elements in the mark matrix L constituted the so-called “watershed line”, the other non-zero elements were marked as the “water basins”, i.e., rust pits. The maximum value p ($p = \max(\max(L))$) of the elements in the mark matrix L represented the total number of the identified rust pits.

$$L = \text{watershed}(B(x, y)) \quad (5)$$

Step 6: Rust pit extraction. The `For` loop, `Find(L == k)` function (where $k \in 1 : \max(\max(L))$) and the contour extraction function `Bwperim` were applied to find the marking elements of the arbitrary k -th rust pit in the mark matrix L and return the index value. Furthermore, the position coordinates X_i and Y_i of all the scanning points in k -th rust pit in the topographic matrix T could be obtained using the index value, and then the Z_i value of the corresponding point in the topographic matrix T could be acquired according to the position coordinates X_i and Y_i . Consequently, the rust pit matrix C_k and the contour matrix D_k for the arbitrary k -th rust pit could be obtained.

3.2. Method of Calculating the Size and Shape of Rust Pits

Figure 5 presents the calculation diagram for the shape and size of rust pits. According to the above rust pit identification and extraction method, the rust pit matrix C_k for the arbitrary k -th rust pit could be obtained, assuming it was q rows \times 3 columns, where q represented the total number of scanning points within the range of the k -th rust pit and the 3 columns of matrix C_k stored the X_i , Y_i , and Z_i coordinates of each scanning point, respectively. The size parameters, including the projected area, diameter, and depth of the k -th rust pit, could be calculated based on rust pit matrix C_k .

$$A = q \cdot \lambda_1 \cdot \lambda_2 \quad (6)$$

$$r_1 = \frac{1}{2}(W_X + W_Y) \quad (7)$$

$$d_1 = \max(C_k(:, 3)) - \min(C_k(:, 3)) \quad (8)$$

where A is the projected area of the rust pit; λ_1 and λ_2 are the scanning steps in the width and length directions of the topography scanning area, respectively; q is the rows of matrix C_k and $q = \text{size}(C_k, 1)$; r_1 is the diameter of the rust pit considering the irregularity in the shape of the rust pit, which is taken as the average of the width of the rust pit in both the rolling direction and flange width direction; d_1 is the depth of the rust pit, which is defined as the depth difference between the highest point and the deepest point within the scope of the rust pit; and W_X and W_Y are the width of the rust pit contour in the width and length directions, as shown in Figure 5.

$$W_X = \max(C_k(:, 1)) - \min(C_k(:, 1)) \quad (9)$$

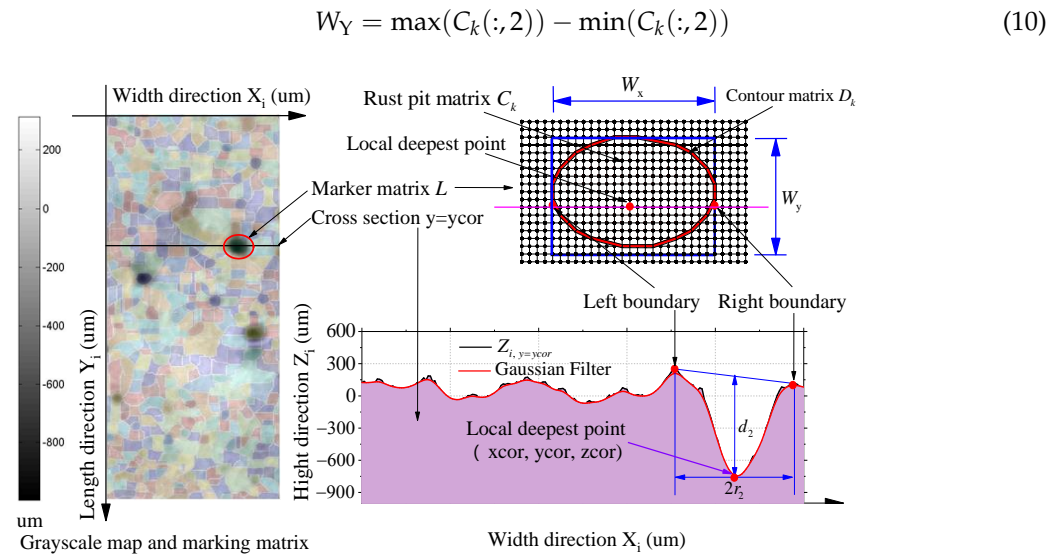


Figure 5. Calculation diagram of shape and size for rust pits.

In addition to the above size parameters, the evaluation method for shape parameters, such as depth diameter ratio D_{R1} , area ratio A_R , and volume ratio V_R , are also calculated as follows:

$$D_{R1} = d_1 / r_1 \quad (11)$$

$$A_R = A / A_C \quad (12)$$

$$V_R = V / V_C \quad (13)$$

where A_C is the minimum rectangular area surrounding the projection area of the rust pit; V is the volume of the rust pit calculated as the sum of the volume of all small prisms within the scope of the rust pit; and V_C is the minimum cuboid volume surrounding the rust pit.

$$A_C = W_X \cdot W_Y \quad (14)$$

$$V = \sum_{i=1}^m (\max(C_k(:,3)) - Z_i) \cdot \lambda_1 \cdot \lambda_2 \quad (15)$$

$$V_C = d_1 \cdot W_X \cdot W_Y \quad (16)$$

The area ratio A_R and volume ratio V_R are important indicators for judging the shape of the projected area of the rust pit and the shape of the rust pit. The area ratios A_R of the (elliptical) circular, triangular, and rectangular projected surfaces are $\pi/4$, $1/2$, and 1, respectively. The volume ratios V_R of semi (elliptical) spheres, cones, and cylinders are $\pi/6$, $\pi/12$ and $\pi/4$, respectively [17].

In view of the fact that, in the fatigue life prediction of corroded steel structures, the size of a rust pit (such as the depth and width of the rust pit) on a section plane that is perpendicular to the tensile direction of a steel plate is generally equivalent to the initial crack size in order to carry out fatigue crack growth analysis. A calculation process for the sectioning depth (d_2), sectioning diameter (r_2), and sectioning depth diameter ratio (D_{R2}) was also proposed:

$$d_2 = \frac{1}{2} \left(\max(D_k(:,3)_{y=y_{cor}}) + \min(D_k(:,3)_{y=y_{cor}}) \right) - \min(C_k(:,3)) \quad (17)$$

$$r_2 = \frac{1}{2} \left(\max(D_k(:,1)_{y=y_{cor}}) + \min(D_k(:,1)_{y=y_{cor}}) \right) \quad (18)$$

$$D_{R2} = d_2 / r_2 \quad (19)$$

where D_k is the contour matrix of the arbitrary k -th rust pit; and $y = y_{cor}$ denotes the profile along the plate width direction and through the local deepest point (x_{cor} , y_{cor} , z_{cor}) in the k -th rust pit, as shown in Figure 5.

4. Results and Discussion

4.1. Rust Pit Density

The extraction results for the pit density and depth of corroded steel plates with different corrosion durations are presented in Table 1. Figure 6 illustrates the variation law of rust pit density with corrosion duration. It can be observed from Figure 6 that the density of rust pits on the surfaces of the corroded steel plates presented a peak value when the corrosion duration was 3 months. With the corrosion duration continuously increasing from 3 months to 4, 6, 8, 12, and 15 months, the density of the rust pits presented a fluctuating change process of first decreasing and then increasing, followed by decreasing and, finally, increasing. To interpret the variation in rust pit density versus corrosion, as shown in Figure 6, of great relevance in the assessment of the effect corrosion duration had on rust pit density was the qualitative analysis of the corrosion reaction process on the surfaces of the steel plates. Figure 7 presents the corrosion morphologies of H-shaped steel corresponding to different corrosion durations. In the early stage of artificial accelerated corrosion, the anodic reaction due to the deposition and adsorption of chloride ions and the formation of localized pitting firstly occurred on the steel surface with defects and impurities. A small amount of bubbles and the corresponding pits appeared on the surfaces of the steel plates, as shown in Figure 7a. When the corrosion duration reached 3 months, the surfaces of the steel plates presented the most significant pitting characteristics: the pits were small and densely distributed, and the rust pit density reached a maximum value. With further increase in corrosion duration (e.g., from 3 months to 4 months), small and dense pits began to connect with each other to form larger pits, and the quantity of pits decreased. Then, a rust layer appeared, and uniform corrosion became more obvious, resulting in a decrease in rust pit density. With the corrosion duration increasing from 4 months to 6 months, the existence of a small amount of loose rust caused pitting corrosion and uniform corrosion on the steel plate surfaces alternately, as shown in Figure 7b. Thus, the variation in pit density was not significant. With the corrosion duration increasing from 6 months to 12 months, loose corrosion products turned dense and hard. The chlorine and dissolved oxygen could hardly reach the bottom of the rust pits due to the increasingly retardation of the rust layer, and thus, the pits grew mainly in the width direction. Therefore, contiguous uniform corrosion was found in Figure 7c, and the rust pit density decreased continually. With further increase in corrosion duration, the rust layer changed from monolayer to multilayer with the accumulation of corrosion products, and the sloughing of the rust layer can be found in Figure 7d. The chlorine and dissolved oxygen could easily reach the surface of the uncorroded metal, so pitting corrosion took the dominant role again, and the rust pit density increased somewhat.

Table 1. Extraction results of pit density and depth for corroded steel plates with different corrosion durations.

Specimen No.	Corrosion Duration/Month	Weight Loss Rate/%	Rust Pit Density /mm ⁻²	Average Pit Depth /μm	Maximum Pit Depth /μm	Median of Rust Pit Depth /μm
C3	3	5.08	59.55	170.21	632.51	155.25
C4	4	6.15	54.65	145.48	417.63	137.14
C6	6	7.92	55.7	150.62	462.16	141.63
C8	8	10.07	52.1	161.36	628.74	142.37
C12	12	15.02	43.35	191.80	493.09	184.04
C15	15	18.09	54.3	185.76	428.90	184.13

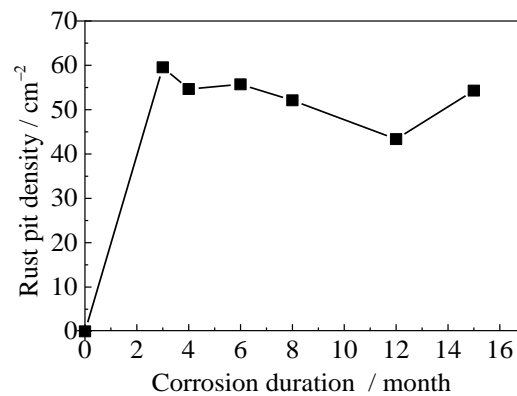


Figure 6. Rust pit density versus corrosion duration.

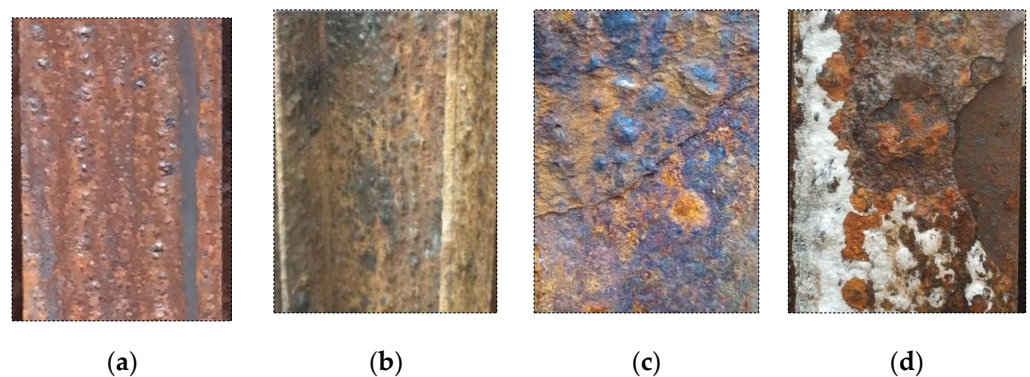


Figure 7. Corrosion morphology of H-shaped steel corresponding to different corrosion durations: (a) 1 month; (b) 6 months; (c) 10 months; (d) 12 months.

4.2. Rust Pit Size

It can be seen from Table 1 that the average pit depth and the median depth of the rust pits both reached a maximum value when the corrosion duration was 3 months; they then decreased with the corrosion duration increase from 3 months to 4 months. With the corrosion duration increasing from 4 months to 15 months, the average pit depth and the median depth of the rust pits increased. The average pit depth and the median depth of the rust pits reflected the general characteristics of the depth of the rust pits, which were also dominated by pitting corrosion and uniform corrosion on the steel surfaces. The maximum values of the average pit depth and median depth appeared at the corrosion duration of 3 months, which again reflected the most significant pitting characteristics on the steel surfaces at the corrosion duration of 3 months. The following fluctuation process of the values for average pit depth and median depth might mainly depend on the alternating dominant role of local pitting corrosion and uniform corrosion during the corrosion process of the steel plates. The maximum pit depth also appeared on the surfaces of the steel plates with a corrosion duration of 3 months. With the corrosion duration gradually increasing from 3 months to 15 months, the maximum pit depth presented a fluctuating process of first decreasing, then increasing, and then decreasing. Figure 8 illustrates the frequency distribution for the pit depth of corroded steel plates with different corrosion durations. It can be found from Figure 8 that, for corroded steel plates with corrosion durations of 3, 4, 6, 8, 12, and 15 months, the distribution widths of the rust pit depth were 0~640 μm , 20~420 μm , 0~480 μm , 20~560 μm , 20~500 μm , and 20~420 μm , respectively. The distribution width of the rust pit depth presented a peak value at the corrosion duration of 3 months and then showed a fluctuating process with further increase in the corrosion duration. The depth ranges of rust pits corresponding to the maximum distribution

frequencies were 140 μm ~160 μm , 120 μm ~140 μm , 120 μm ~140 μm , 120 μm ~140 μm , 140 μm ~160 μm , and 180 μm ~200 μm , respectively.

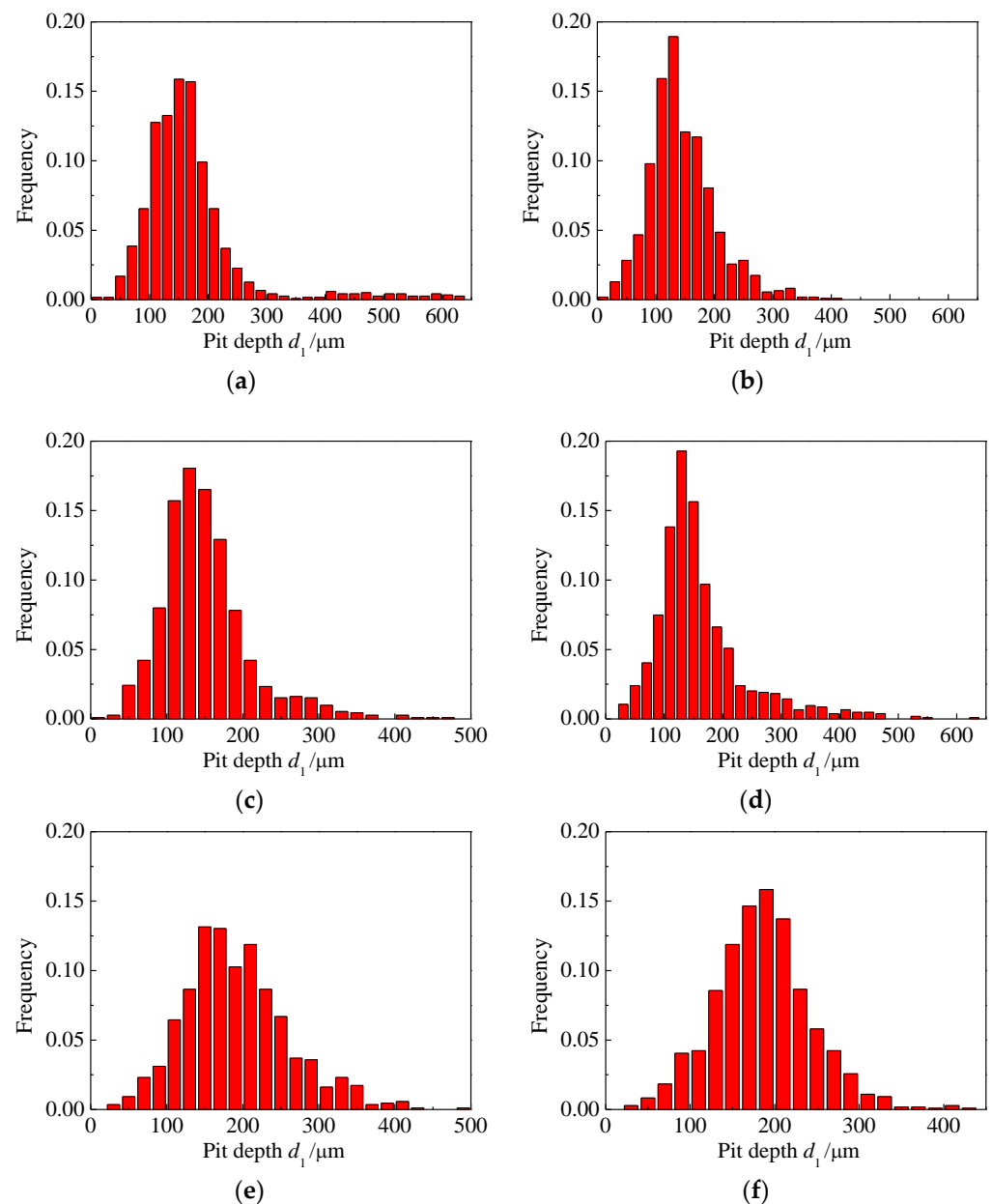


Figure 8. Frequency distributions of pit depths of corroded steel plates with different corrosion durations: (a) C3, (b) C4, (c) C6, (d) C8, (e) C12, (f) C15.

Figure 9 depicts the depth diameter ratio D_{R1} versus the rust pit depth d_1 for corroded steel plates with different corrosion durations. As shown in Figure 9, the depth diameter ratios of the rust pits were mainly distributed in the range of 0.1~0.8. Corrosion duration presented a certain influence on the distribution range of the depth diameter ratios. With the corrosion duration increasing from 3 months to 15 months, the distribution range of the depth diameter ratios of the rust pits roughly decreased at first and then increases, followed by a decrease and, finally, increasing again, which may be related to the alternating dominant role of rust pit growth in the width and depth directions. Except for the C3 specimens, no obvious correlation was found between the depth diameter ratio D_{R1} and the rust pit depth d_1 for specimens with different corrosion durations. The width distribution and depth distribution of the rust pits were independent of each other. The depth diameter

ratio of the rust pits on specimen C3 approximately increased with the increase in rust pit depth, which may be related to the significant pitting phenomenon on the surface of the C3 specimen at an early stage of artificially accelerated corrosion.

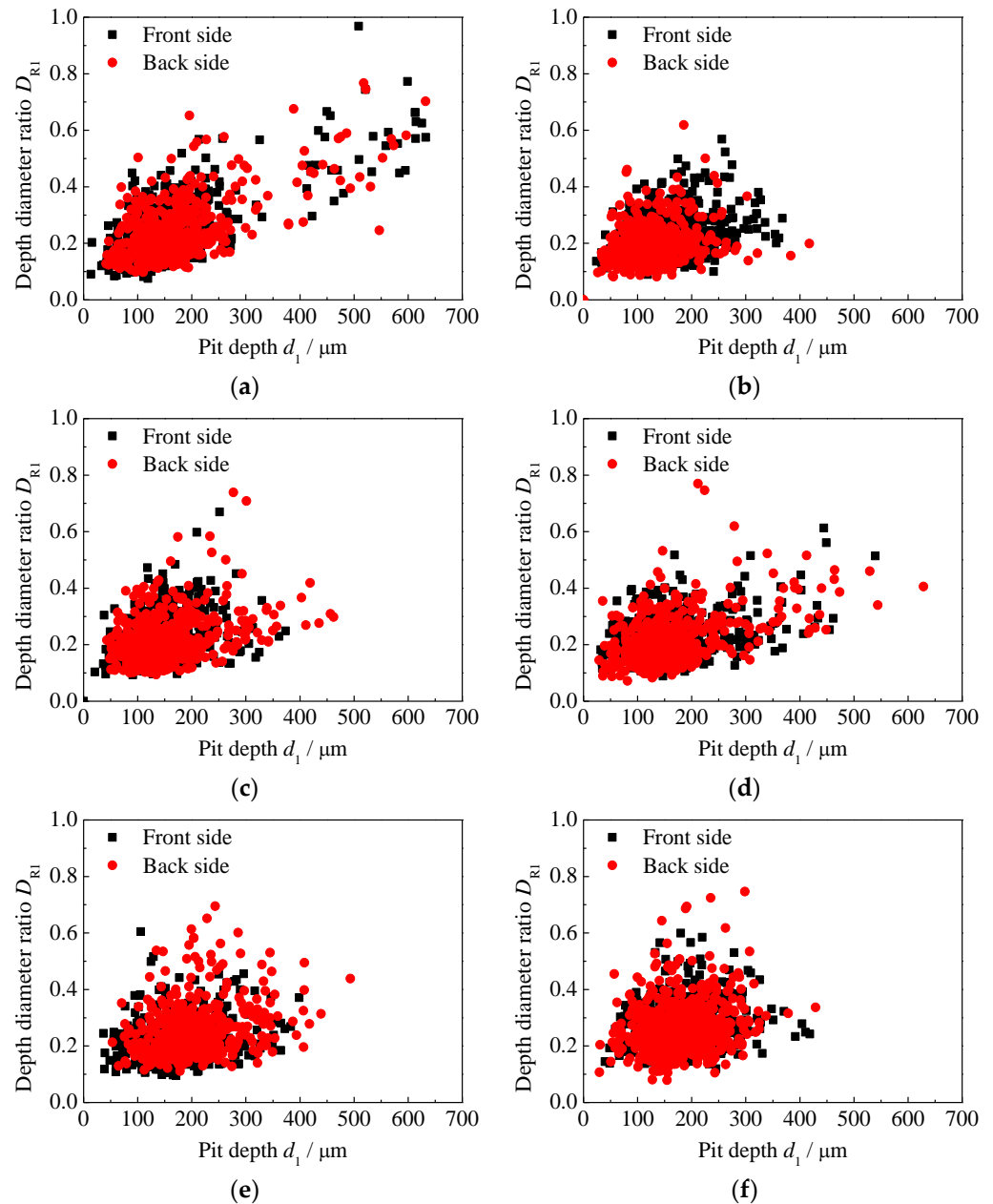


Figure 9. Depth diameter ratio D_{R1} versus rust pit depth d_1 for corroded steel plates with different corrosion durations: (a) C3, (b) C4, (c) C6, (d) C8, (e) C12, (f) C15.

4.3. Rust Pit Shape

Figure 10 presents the rust pit depth d_1 versus volume ratio V_R , as well as the frequency distribution of V_R , for corroded steel plates with different corrosion durations. It can be found from Figure 10 that, for specimens with different corrosion durations, the volume ratios V_R of rust pits were mostly between $\pi/12$ and $\pi/4$. The volume ratio corresponding to the peak frequency was around $\pi/6$, indicating that most rust pits were similar to semi (ellipsoidal) spheres in shape. There was no obvious correlation between the volume ratio V_R and the rust pit depth d_1 , indicating that the shape distribution of the rust pits did not change significantly with rust pit depth. As far as the distribution range of rust

pit depth was concerned, specimen C3 presented the widest distribution range for rust pit depth, followed by specimen C8, and there were no obvious differences between the other specimens. When the rust pit depth remained unchanged, the “sharpness” of the cylinder rust pits, half (ellipsoidal) sphere rust pits, and cone rust pits increased in turn. The volume ratios V_R for the critical pits (i.e., the deepest rust pits) of specimens C3 and C15 were mostly concentrated around $\pi/12$ (cone rust pit) and $\pi/6$ (half (ellipsoidal) sphere), respectively. The volume ratios V_R for the critical pits of specimens C4, C6, and C12 were between $\pi/12$ (cone rust pit) and $\pi/6$ (half (ellipsoidal) sphere), while the volume ratios V_R for the critical pits of specimen C8 were between $\pi/6$ (half (ellipsoidal) sphere) and $\pi/4$ (cylinder rust pit).

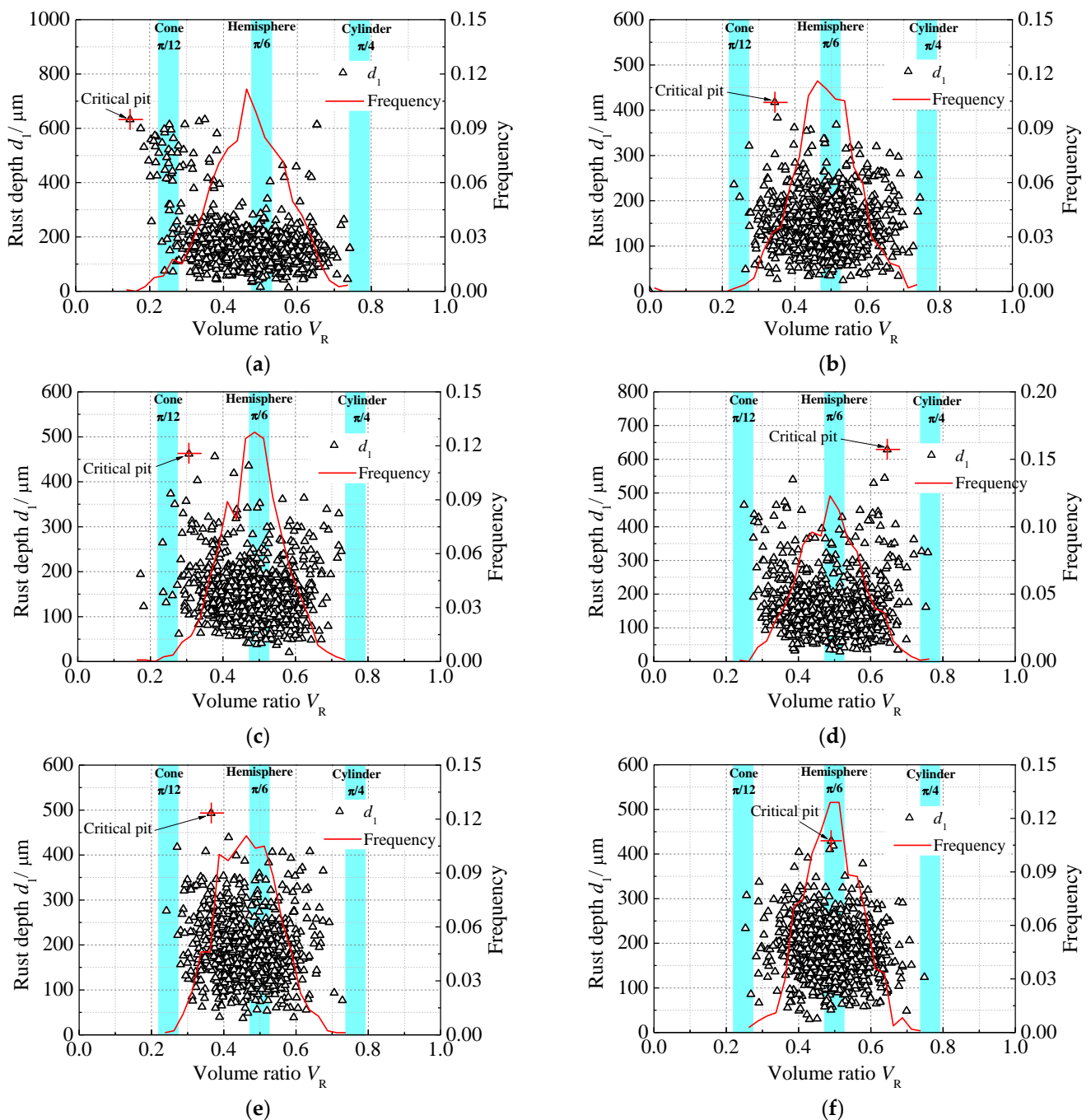


Figure 10. Rust pit depth d_1 versus volume ratio V_R , as well as the frequency distribution of V_R , for corroded steel plates with different corrosion durations: (a) C3, (b) C4, (c) C6, (d) C8, (e) C12, (f) C15.

5. Conclusions

In the present study, a new method for the identification, extraction, and evaluation of rust pits on the surfaces of corroded steel structures was proposed by combining three-dimensional topography-scanning technology and a watershed image segmentation algorithm with which the size and shape parameters of rust pits could be quickly and accurately extracted. The statistical analysis of the extraction results for the rust pits of corroded steel plates subjected to accelerated corrosion showed that rust pit density had a peak value at the corrosion duration of 3 months, and rust pit density showed a fluctuating process with corrosion duration, which continually increased from 3 months to 15 months. The values of the depth diameter ratios of rust pits were concentrated in the range of 0.1~0.8. With corrosion duration increasing from 3 months to 4, 6, 8, 12, and 15 months, the distribution range of the depth diameter ratios of rust pits decreased at first and then increased, followed by a decrease and, finally, an increase. The width distribution of rust pits was independent from the depth distribution of rust pits. The values of the volume ratios were mostly distributed between $\pi/12$ and $\pi/4$, and the shapes of most rust pits were similar to half (ellipsoidal) spheres. The outcomes of this study can provide meaningful references and essential data for the fatigue performance evaluation of existing corroded steel structures.

Author Contributions: Conceptualization, A.L.; methodology, A.L.; software, A.L. and H.M.; validation, A.L.; formal analysis, A.L.; investigation, A.L. and H.M.; resources, A.L.; data curation, A.L. and H.M.; writing—original draft preparation, A.L.; writing—review and editing, all authors; visualization, A.L.; supervision, S.X.; project administration, A.L. and S.X.; funding acquisition, A.L. and S.X. All authors have read and agreed to the published version of the manuscript.

Funding: This research was funded by the National Natural Science Foundation of China (No. 52008331), the China Postdoctoral Science Foundation (No. 2021MD703867), the Shaanxi Provincial Key Research and Development Program (No. 2022SF-467), the Independent Research and Development Project of State Key Laboratory of Green Building in Western China (No. LSZZ202114), and the Key Scientific Research Projects of Shaanxi Provincial Department of Education (No. 21JS030).

Data Availability Statement: Not applicable.

Conflicts of Interest: The authors declare no conflict of interest. The funders had no role in the design of the study; in the collection, analyses, or interpretation of data; in the writing of the manuscript; or in the decision to publish the results.

References

1. Xu, S.; Wang, H.; Li, A.; Wang, Y.; Su, L. Effects of corrosion on surface characterization and mechanical properties of butt-welded joints. *J. Constr. Steel Res.* **2016**, *126*, 50–62. [\[CrossRef\]](#)
2. Wang, Y.; Zhou, X.; Wang, H.; Kong, D.; Xu, S. Stochastic constitutive model of structural steel based on random field of corrosion depth. *Case Stud. Constr. Mater.* **2022**, *16*, e00972. [\[CrossRef\]](#)
3. Li, A.; Xu, S.; Wang, Y.; Wu, C.; Nie, B. Fatigue behavior of corroded steel plates strengthened with CFRP plates. *Constr. Build. Mater.* **2022**, *314*, 125707. [\[CrossRef\]](#)
4. Li, A. Fatigue Behavior and Design Method of Corroded Steel Plate Strengthened with CFRP Plates. Ph.D. Thesis, Xi'an University of Architecture & Technology, Xi'an, China, 2020.
5. Cerit, M. Numerical investigation on torsional stress concentration factor at the semi elliptical corrosion pit. *Corros. Sci.* **2013**, *67*, 225–232. [\[CrossRef\]](#)
6. Xu, S.-H.; Qiu, B. Experimental study on fatigue behavior of corroded steel. *Mat. Sci. Eng. A-Struct.* **2013**, *584*, 163–169. [\[CrossRef\]](#)
7. Xu, S.H.; Wang, Y.D. Estimating the effects of corrosion pits on the fatigue life of steel plate based on the 3D profile. *Int. J. Fatigue* **2015**, *72*, 27–41. [\[CrossRef\]](#)
8. Dolley, E.J.; Lee, B.; Wei, R.P. The effect of pitting corrosion on fatigue life. *Fatigue Fract. Eng. Mater. Struct.* **2000**, *23*, 555–560. [\[CrossRef\]](#)
9. Duquesnay, D.L.; Underhill, P.R.; Britt, H.J. Fatigue crack growth from corrosion damage in 7075-T6511 aluminium alloy under aircraft loading. *Int. J. Fatigue* **2003**, *25*, 371–377. [\[CrossRef\]](#)
10. Zhang, C.; Yao, W.X. Judgment of critical pits and calculation of fatigue life. *J. Mech. Strength* **2013**, *35*, 207–213.
11. Sankaran, K.K.; Perez, R.; Jata, K.V. Effects of pitting corrosion on the fatigue behavior of aluminum alloy 7075-T6: Modeling and experimental studies. *Mater. Sci. Eng. A* **2001**, *297*, 223–229. [\[CrossRef\]](#)

12. Li, A.B.; Wang, H.; Li, H.; Kong, D.L.; Xu, S.H. Stress Concentration Analysis of the Corroded Steel Plate Strengthened with Carbon Fiber Reinforced Polymer (CFRP) Plates. *Polymers* **2022**, *14*, 3845. [[CrossRef](#)] [[PubMed](#)]
13. Holme, B.; Lunder, O. Characterisation of pitting corrosion by white light interferometry. *Corros. Sci.* **2007**, *49*, 391–401. [[CrossRef](#)]
14. Pidaparti, R.M.; Patel, R.R. Correlation between corrosion pits and stresses in Al alloys. *Mater. Lett.* **2008**, *62*, 4497–4499. [[CrossRef](#)]
15. Wang, Y.; Cheng, G. Quantitative evaluation of pit sizes for high strength steel: Electrochemical noise, 3-D measurement, and image-recognition-based statistical analysis. *Mater. Des.* **2016**, *94*, 176–185. [[CrossRef](#)]
16. Tang, F.; Lin, Z.; Chen, G.; Yi, W. Three-dimensional corrosion pit measurement and statistical mechanical degradation analysis of deformed steel bars subjected to accelerated corrosion. *Constr. Build. Mater.* **2014**, *70*, 104–117. [[CrossRef](#)]
17. Codaro, E.N.; Nakazato, R.Z.; Horovistiz, A.L.; Ribeiro, L.M.F.; Ribeiro, R.B.; Hein, L.R.O. An image processing method for morphology characterization and pitting corrosion evaluation. *Mat. Sci. Eng. A-Struct.* **2002**, *334*, 298–306. [[CrossRef](#)]
18. Walde, K.V.D.; Hillberry, B.M. Characterization of pitting damage and prediction of remaining fatigue life. *Int. J. Fatigue* **2008**, *30*, 106–118.
19. Wang, Y.; Xu, S.; Wang, H.; Li, A. Predicting the residual strength and deformability of corroded steel plate based on the corrosion morphology. *Constr. Build. Mater.* **2017**, *152*, 777–793. [[CrossRef](#)]
20. Beucher, S. Use of watersheds in contour detection. In Proceedings of the International Workshop on Image Processing: Real-Time Edge and Motion Detection, Rennes, France, 17–21 September 1979.
21. Vincent, L.; Soille, P. Watersheds in digital spaces: An efficient algorithm based on immersion simulations. *IEEE Trans. Pattern Anal.* **1991**, *13*, 583–598. [[CrossRef](#)]
22. De Smet, P.; Pires, R.L.V. Implementation and analysis of an optimized rainfalling watershed algorithm. In *Image and Video Communications and Processing 2000*; International Society for Optics and Photonics: San Jose, CA, USA, 2000; pp. 759–767.
23. Zhang, J.; Feng, W.; Hu, C.; Luo, Y. Image segmentation method for forestry unmanned aerial vehicle pest monitoring based on composite gradient watershed algorithm. *Trans. Chin. Soc. Agric. Eng.* **2017**, *33*, 93–99.
24. Wu, X.; Liao, Y.; Fan, Y.; Cheng, F. Segmentation of Pork Longissimus Dorsi Based on KFCM Clustering and Improved Watershed Algorithm. *Trans. Chin. Soc. Agric. Mach.* **2010**, *41*, 172–176.
25. Tong, Z.; Pu, L.; Dong, F. Automatic segmentation of clustered breast cancer cells based on modified watershed algorithm and concavity points searching. *J. Biomed. Eng.* **2013**, *30*, 692–696.
26. Song, L.W.; Song, C.Y.; Zhuang, T.G. Watershed-Based Brain Magnetic Resonance Image Automated Segmentation. *J. Shanghai Jiaotong Univ.* **2003**, *37*, 1754–1756.
27. Cai, H.Y.; Yao, G.Q. Optimized method for road extraction from high resolution remote sensing image based on watershed algorithm. *Remote Sens. Land Resour.* **2013**, *25*, 25–29.
28. Zhang, B.; He, B.B. Multi-scale segmentation of high-resolution remote sensing image based on improved watershed transformation. *J. Geo-Inform. Sci.* **2014**, *16*, 142–150.
29. Fang, Y.; Yang, X.C.; Lei, J.B. Research on shallow spot defect detection based on laser remanufacturing robot. *Chin. J. Lasers* **2012**, *39*, 1203005. [[CrossRef](#)]
30. Lan, H.; Fang, Z.Y. Image recognition of steel plate defects based on a 3D gray matrix. *J. Image Graph.* **2019**, *24*, 859–869.
31. Xiaoguang, Z.; Zheng, S.; Xiaolei, H. Extraction method of welding seam and defect in ray testing image. *Trans. China Weld. Inst.* **2011**, *32*, 77–80.
32. *GB/T 24517-2009*; Corrosion of Metals and Alloys, Outdoors Exposure Test Methods for Periodic Water Spray. Standards Press of China: Beijing, China, 2009.
33. *GB/T 10125-2012*; Corrosion Tests in Artificial Atmospheres—Salt Spray Tests. Standards Press of China: Beijing, China, 2012.